Oral presentation | Aero-acoustics
Aero-acoustics-II
Mon. Jul 15, 2024 2:00 PM - 3:30 PM Room B

[2-B-02] Wall Modelled Large Eddy Simulation for Jet Flap Interaction Aeraocoustics

*Gary Page[1], Hao Xia[1], Andrew Barnes[1], Simran Panesar[1] （1. Loughborough University）

Keywords: Jet Noise, Wall Modelled Large Eddy Simulation, Aeroacoustics

Twelfth International Conference on
Computational Fluid Dynamics (ICCFD12),
Kobe, Japan, July 14-19, 2024

Wall Modelled Large Eddy Simulation for Jet Flap Interaction Aeroacoustics

G.J. Page, H. Xia, A. Barnes and S. Panesar
Corresponding author: g.j.page@lboro.ac.uk
Dept. of Aeronautical and Automotive Engineering,
Loughborough University, LE11 3TU. UK

Abstract: With the move towards higher bypass ratio turbofans on transport aircraft to improve efficiency, the large diameter makes them challenging to install under the wing. One unintended consequence is that the trailing edge of a deployed flap may now interact with the propulsive jet stream creating a significant noise source (Jet Flap Interaction). CFD simulations are reported for Wall Modelled LES of a simplified wing/flap/nacelle geometry and a realistic aircraft geometry with a modern engine installation. The simplified geometry showed that WMLES on modest grids is capable of resolving realistic turbulent structures and gives a clear increase in noise when the flap is deployed. Despite the experimental data having a significant rig noise component, comparison between simulation and experimental noise increments was reasonable for both the near and mid field measurements. The same methodology and grid design was applied to a High Lift Common Research Model in a Take Off configuration that included a realistic nacelle, intake and jet flow. Jet Flap Interaction was observed in simulated shadowgraphs. Virtual probes on the fuselage showed that an above wing microphone is likely to be contaminated by airframe noise and it is recommended to be placed under the wing to measure jet noise.

Keywords: Computational Fluid Dynamics, Aeroacoustics, Jet Noise, Large Eddy Simulation

1 Introduction

To reduce CO_2 emissions of transport aircraft, the engine bypass ratio can be increased to improve the propulsive efficiency and so reduce fuel burn. However, installation of these large diameter Ultra High Bypass Ratio (UHBR) turbofan engines can be challenging as they are installed even closer to the wing to avoid excessive undercarriage leg lengths. This can result in both aerodynamic performance penalties and a risk of increased noise. The concern is that the trailing edge of a deployed flap will interact with the turbulent jet plume resulting in a strong noise source known as Jet Flap Interaction (JFI). In the past, industry has used testing of subscale isolated jets in anechoic facilities to provide data to calibrate aircraft noise models. But, with the requirement to now include the airframe in the testing it can be difficult to achieve the correct flight conditions – and unfortunately many of the anechoic facilities have closed down. This work, as part of the ODIN (Off-Design Installed Nacelles) European Union Clean Sky 2 project[1], investigates whether the combination of installed jet noise testing within an aerodynamic, non-anechoic wind tunnel (concurrent with propulsion aerodynamic testing) and a proposed full scale flight test aircraft could be used to reduce the risk of Jet Flap Interaction and to provide quantitative input to aircraft noise models.

This work builds upon previous experimental [1] and computational [2] studies of Jet Flap Interaction and utilises recent advances in the use of Wall Modelled Large Eddy Simulation [3] to resolve turbulence on both the airframe and the jet.

Non-anechoic experimental tests for a simplified installed jet geometry were carried out at low speed (representing take off) and at high speed (representing cruise). The CFD simulations were carried out prior to testing and were used to both help support the rig design and test programme and to help assess the validity of the aeroacoustic measurements. A key risk of the testing is the background noise and reverberations in the experiment. The CFD was set up to avoid any reflections from the side and top walls, and of course does not have any rig noise from fans etc. Hence, assuming that the CFD is of sufficient resolution, differences help indicate where the experimental measurements may be contaminated. The CFD is only designed to resolve up to a given Strouhal number, and so above this value we would expect the CFD acoustics levels to be of a lower magnitude.

[1]Project number: 101007598

The work then proceeds by taking the CFD simulation best practices determined in the simplified test case and applying them to a realistic installed aircraft problem in both take off and cruise conditions. This helps to determine if the aerodynamic non-anechoic testing can be carried across to an inflight test case. In addition, the use of virtual probes on the aircraft allows an assessment of appropriate microphone locations in a future flight test programme.

2 Simplified Geometry

Figure 1: Aircraft Research Association Transonic Wind Tunnel installation

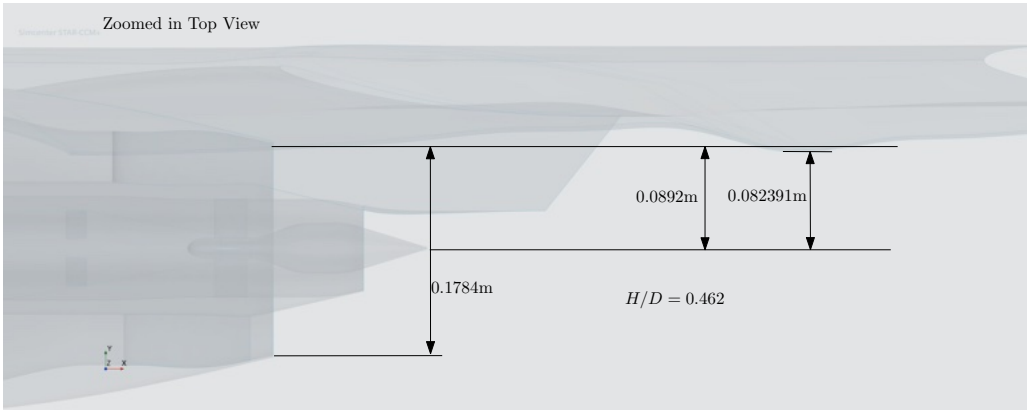

Figure 2: Installation parameters

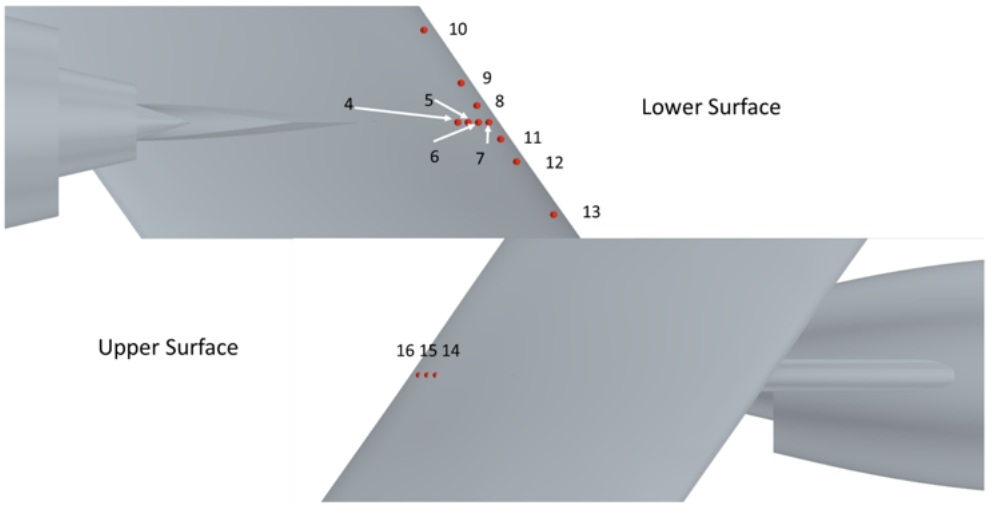

Figure 3: Kulite locations

2.1 Experimental Configuration

The experimental data was taken in the Aircraft Research Association (ARA) Dual Stream Jet Propulsion (DSJP) rig that is based on the AIAA Dual Separate Flow Reference Nozzle. This facility is primarily used for measurement of subscale exhaust nozzle performance and is representative of high bypass ratio turbofans.

For this testing, which is aimed at aeroacoustic assessment, it is used in an installed configuration with a wing as shown in Figure 1. It should be noted that the alignment of the rig does not match a typical aircraft or half-aircraft configuration, here the rig is effectively rotated 180° from the common floor-mounted half-aircraft configuration and no fuselage included. Aligned with the typical backward sweep of aircraft wings, the wing tip towards the roof is equivalent to the inboard or cabin side, whilst the joint between the wing and the floor is equivalent to the outboard side. Two wing models were used, one with a flap deployed at an angle of 20 degrees for Take-off and Approach conditions, and a wing model with the flap undeployed at an angle of 0 degrees for Cruise and Jet-Flap Interaction baseline conditions. The diameter of the bypass exit was 0.1784m. A key parameter is the vertical location of the trailing edge of the flap in relation to the jet axis. When non-dimensionalised by the bypass diameter, a value below 0.5 has the flap TE intersecting the lipline from the bypass. As can be seen in Figure 2 this value of H/D is 0.462 so we would expect a strong jet flap interaction.

The DSJP is used in ARA's Transonic Wind Tunnel (TWT). The TWT is a continuous, closed-circuit wind tunnel with perforated walls giving a 22% open area ratio. The wind tunnel has a test section of 2.74m wide by 2.44m high and can operate at freestream Mach numbers from 0 to 1.4, with stagnation pressures of 0.8 to 1.2bar. It typically operates at ambient pressure and temperature. Perforated walls are used to reduce wall interference by drawing off a portion of the boundary layer. In transonic wind tunnels this helps to minimize shock reflections which can bounce back towards the model and further affect the flow field. For all of the aeroacoustics testing, matched fan and core velocities were used (equivalent to nozzle pressure ratios with a nominal range of 1.28 to 2.6), and reported here as ideal fully expanded jet Mach numbers.

Kulite probes are located near the trailing edge of the wing (Figure 3) to measure the JFI sources and a microphone line array (Figure 4) is mounted on the floor to measure the mid-field propagation of the jet noise.

The Kulite probes are able to resolve the high pressure fluctuations at high frequency that would be expected from the edge of the energetic turbulent jet grazing the flap. (Indeed, the CFD was used to estimate the fluctuations in order to purchase the Kulite model that matched). These fluctuations represent the source of the jet flap interaction and if the CFD cannot correctly predict the source then it cannot ever predict the far-field noise. By the time the pressure fluctuations have reached the floor, their magnitude will have dropped considerably and it is feasible to measure the fluctuations using relatively standard microphones. These microphones are intended to give an indication of jet noise that will reach a far-field observer. However, they are only about 7 secondary diameters from the jet centreline whereas far-field arrays are normally at least 30 diameters, and they are placed on a solid wall which increases the observed signal. For the cruise case (where we are not concerned with far-field noise), these locations are similar to the side of the fuselage and would be important for cabin noise.

Tests were carried out at low speed Take Off conditions (freestream Mach 0.25) and at high speed cruise conditions (freestream Mach 0.85) with realistic nozzle pressure ratios, but the main focus of this work is on the low speed Take Off condition.

2.2 CFD Geometry and Mesh

Two geometries were used for the CFD, consisting of a zero degree flap CAD geometry and a 20 degree flap CAD geometry. These were encased in a flow domain measuring 18m streamwise by 7.2m horizontal by 8.9m vertical, with the nose tip of the rig placed 3m from the inlet. In Figure 4 the light blue lines show the larger CFD domain, whilst the red box is the more confined wind tunnel working section. Since the wind tunnel sidewalls are perforated to relieve pressure it was felt that a larger CFD domain would be preferable to attempting to model the perforated walls. A total of six meshes were produced for the main simulations, three for each geometry representing coarse, medium and fine levels of refinement, corresponding to approximately 10 million, 50 million, and 100 million cells respectively. The increasing level of refinement was focused on the propagation zone from the jet to the microphones as well as the jet mixing region. The same mesh was used for all freestream and jet Mach numbers. As the mesh was designed for Wall Modelled LES , it used large near wall y^+ values resulting in a maximum of $y^+ = 70$ in the most important areas for the flow problem at M=0.85, FNPR=2.6, and up to $y^+ = 451$ on the nose

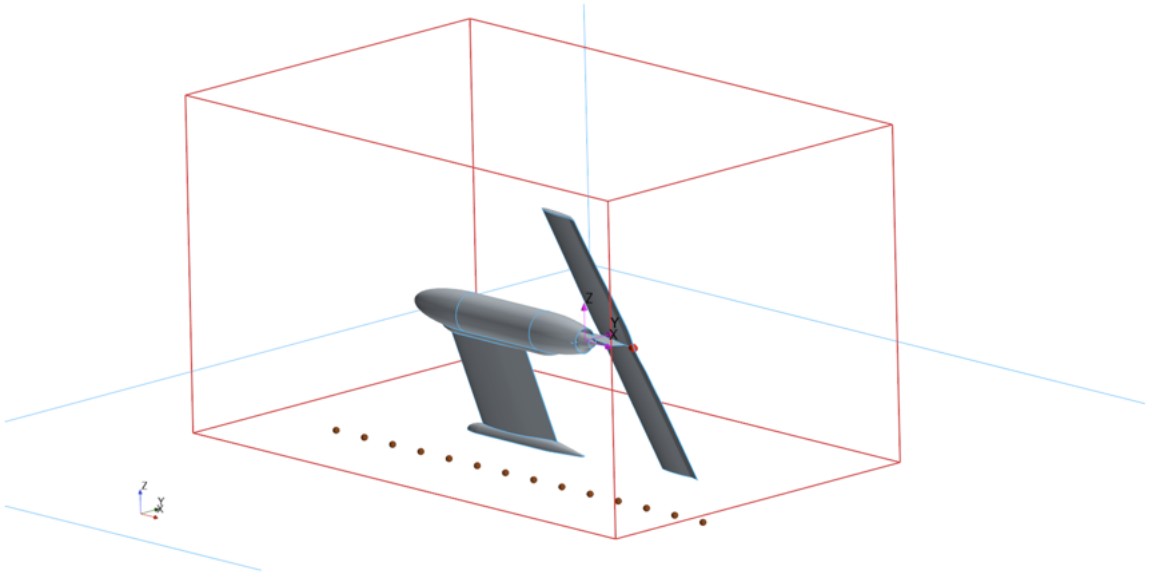

Figure 4: Wind tunnel and CFD domain

of the wall fairings. The meshes also use low aspect ratio cells which are a requirement for WMLES. Anisotropic quadrilaterals were used on the surface and the mesh has been carefully refined at the critical trailing edges utilising the anisotropic feature to cluster in the streamwise direction. (Figure 5)

Prism layers were grown from these surfaces using an Advancing Layer Mesher and connected to polyhedral cells in the core. These polyhedral cells were controlled by wake refinement regions downstream of the nozzle trailing edges to resolve the jet mixing (Figure 6). For the 10 million cell mesh, the smallest cell downstream of the secondary trailing edge in the refinement zone is 0.75% of the secondary diameter, whilst the smallest cells on the trailing edge are 0.185% of the secondary diameter. To propagate acoustic waves from the unsteadiness in the jet to the microphone array, an additional refinement zone was created (Figure 6d). The cells in this zone have a size of 5% of the secondary diameter and this was determined based upon being able to propagate waves with a frequency up to at least a Strouhal number (St) of 1.2 at 20 points per wavelength. Due to the careful use of refinement zones, this initial mesh only contains 10 million cells, yet still captures the key unsteady features of the problem. A refined mesh with 50M cells for validation was then created to resolve up to St=2.4 by halving the cell size in the acoustic refinement zone, alongside other refinements including cells downstream of the secondary trailing edge reducing to 0.275% of secondary diameter and a trailing edge cell size of 0.14% of secondary diameter. The final 100M meshes were a compromise of accuracy and computational cost and increased the resolvable Strouhal number up to 2.8.

2.3 Numerical Parameters

Siemens Simcenter Star-CCM+ 17.02.008 solver was used to run all the current calculations. WMLES was used due to previous experience of accurate predictions for jet noise using relatively coarse meshes, enabling high fidelity simulations to be completed in much shorter periods of time, therefore allowing a more ambitious testing schedule with acceptable computation resources. The WALE subgrid scale model was used with Spalding's wall functions that use off wall information. An implicit unsteady second order time integration formulation was employed and for the spatial discretisation scheme a blend of 5% upwind and 95% central differencing was used.

For the coarse 10M cell mesh a time step δt of 2.5×10^{-6} seconds was used based on achieving Courant number unity for the smallest volumes in the domain. This corresponds to a resolved Strouhal number of 13.9 using 20 points per wavelength in time. For the finer meshes the smallest volume dimension was used to reduce the time step appropriately. A complete simulation using the 10M mesh requires approximately 16,000 core hours running on two 40 core nodes on a local HPC cluster, corresponding to about 8.5 days of elapsed time. For the 50M mesh, approximately 240,000 core hours was required on the same cluster using five 40 core nodes.

Typical jet noise calculations wrap the jet noise sources in a Ffowcs-Williams Hawking (FWH) surface and propagate these to a far-field observer using a Green function. Here, we must directly propagate the

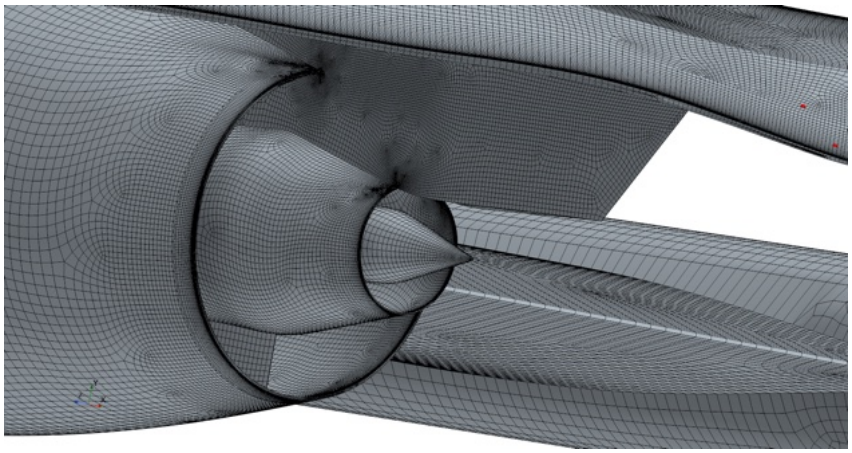

(a) nozzle, pylon and wing

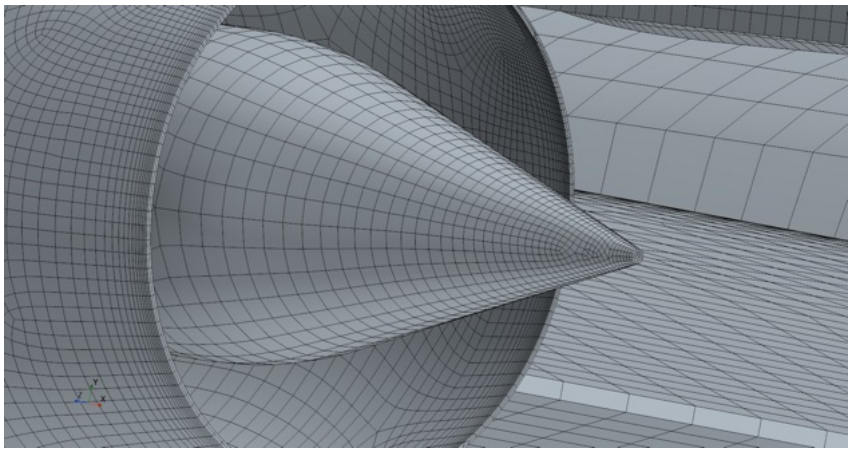

(b) primary stream trailing edge and bullet

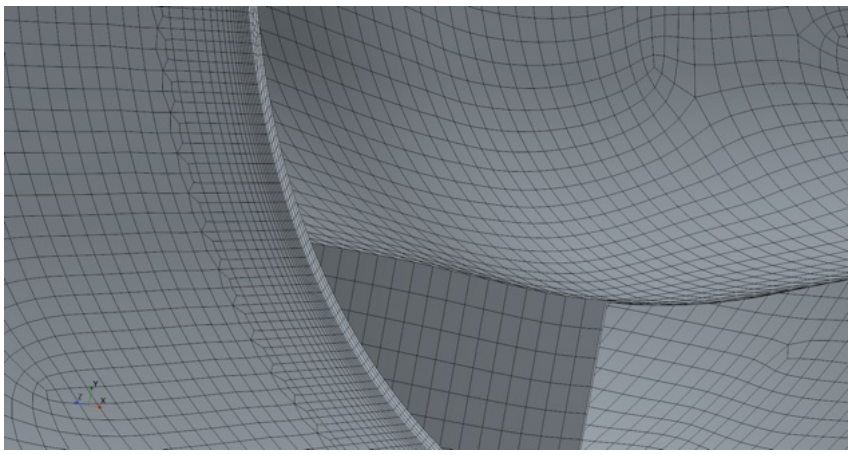

(c) secondary stream trailing edge

Figure 5: Surface mesh on simplified geometry

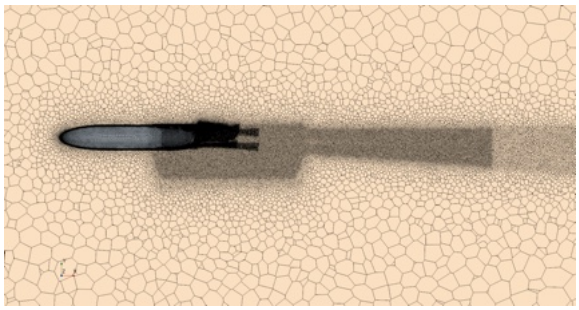

(a) overall

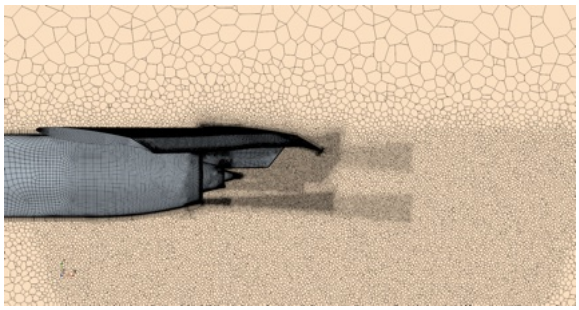

(b) intermediate

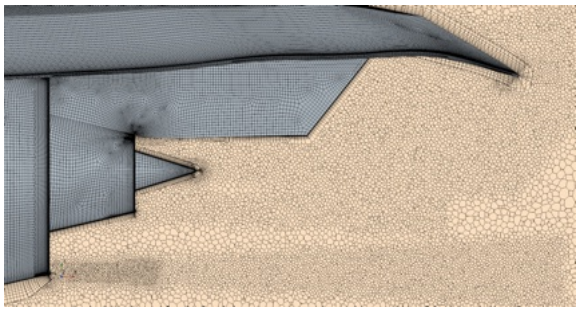

(c) nozzle and flap

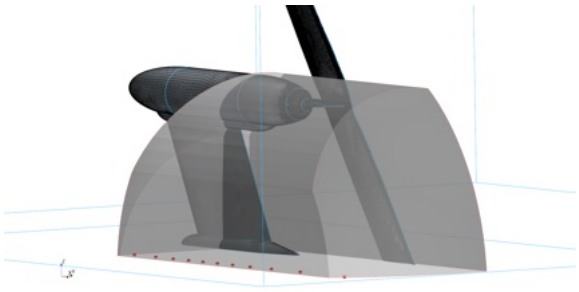

(d) propagation volume refinement

Figure 6: Volumetric mesh refinement

acoustic waves within the CFD solution to microphones in the mid-field. The combination of numerical discretization and mesh spacing will lead to dissipation of waves above a given frequency and so the mesh must be fine in this region.

Within the area of computational aeroacoustics (CAA), the coarsest mesh is sufficient to resolve jet noise to a Strouhal number (St) of 1.2, whilst the finest mesh could resolve up to St=2.8, both being beyond the expected range for jet-flap interaction of 0.1 to 1.0. To resolve St=0.1, a sufficiently long sampling time is required in order to capture the low frequency emissions at the sampled locations. The required sampling time to prevent changes in the results of the CFD was 0.16s, equivalent to 22 periods of the lowest frequency targeted for the study, St=0.1. Running for fewer periods would cause changes in the results around St=0.1, whilst running for longer did not. Due to the small time steps required for LES, the effective sampling rate was 400kHz. To accelerate the transient part of the calculation before we reach a statistical steady state where we take acoustics measurement, a variable time stepping strategy was used. This used a macro that initially computed 5,000 time steps at $5 \times 10^{-}5$ s, then gradually reduced to 5×10^{-6} s. 10,000 time steps were then run at the coarse grid time step of 2.5×10^{-6} s , then for the medium and fine grids ran 15,000 steps at their further reduced time.

Overall, 23 LES solutions were computed, with six of these being on the medium (56M) mesh and two on the fine (100M) mesh. These were predominantly for the freestream Mach number of 0.2, with fully expanded jet Mach numbers of 0, 0.2, 0.6 and 0.9. The jet switched off case allowed comparison to the model in the tunnel with the wind on and jet off, whilst the Mach 0.2 jet case was designed to match the freestream Mach 0.2 to assess the airframe noise. Some cases were also run for freestream Mach 0.3, 0.80 and 0.85 with Nozzle Pressure Ratios up to 2.6.

2.4 Overall Flow Field and Mesh Dependency

Computational Fluid Dynamics will always trade off accuracy and computational resource requirements. The Wall Modelled LES is considerably more expensive than RANS for a given grid (by about one order of magnitude), and there is also more than an order of magnitude difference in cost between the coarse 10M cell calculations and the finest 100M cell calculations. Normally, 10M cells would be deemed too coarse to be useful for LES. However, the careful mesh design and large near wall spacing means that these coarse cases give reasonable results and were used to explore the range of test parameters, with the 50M and 100M cell cases being used for key conditions. This section shows the compromise between the grid sizes and how they affect different flow quantities of interest. The impact on the acoustic results

will be shown in a later section.

Figure 7 shows instantaneous slices of Mach number and the interaction of the flap with the jet flow. It is clear that as the mesh is refined more fine scale turbulence is captured (this is particularly important in the initial jet shear layer) but the overall flow structure is very similar. Although not shown here, the mean flow is almost indistinguishable. Whilst the flap does not directly protrude into the high speed core of the jet, it does deflect the bulk flow downwards. This simplified geometry has a *plain* flap at 20 degrees (unlike a real aircraft that has a slot to energise the top surface boundary layer) and the flow is close to separation on the top surface. Although the 50M cell and 100M cell results look similar, this is not sufficient to argue that the case is sufficiently well resolved as the resolvable length scale only differs by approximately $\sqrt[3]{100/50} \approx 1.26$.

The Q-criterion parameter is useful to understand the resolution of vortical structures. Figure 8 shows how even the coarsest mesh using Wall Modelled LES successfully resolves the larger turbulent structures on the forebody and wing of the rig geometry so providing realistic boundary conditions to the downstream jet flow. Part of the reason for the relatively small differences is that much of the mesh refinement is focussed on the jet and the propagation between the jet and the floor (right hand side of these figures). The lack of mesh resolution downstream of the outboard wing section means that these structures rapidly decay. This can be seen more clearly in Figure 9 where the wake from the upstream nacelle mount is well resolved. It is noteable how the turbulence in the nacelle boundary layer smoothly blends into the jet shear – Detached Eddy Simulation would show a jump here from RANS to LES mode.

2.5 Noise Sources

Figure 10 shows the pressure fluctuations by subtracting the instantaneous pressure field from the long time averaged mean. Even at this reduced scale of +/-1kPa these are predominantly hydrodynamic pressure fluctuations that do not propagate to the far field. However, the larger spots of alternating pressure on the underside of the trailing edge of the flap in Figure 10b is the source of Jet Flap Interaction. An even tighter scale on pressure shows the propagating noise in Figure 11a where the lower frequencies are clearly emanating from the flap trailing edge. Figure 11b rotates the view so that the wing is now vertical and the slice is positioned through the microphone locations - one set of circular waves is emanating from the trailing edge and their reflection from the solid wall sets up an interference pattern.

2.6 Acoustic Results

Before progressing on to examine Jet Flap Interaction and comparison with experimental data it is important to determine how the different mesh resolution affects the noise signal at the near field Kulites and the mid-field microphones. Figure 12 compares the three mesh resolutions for the Power Spectral Density predicted on the wing underside (Kulite 4) and at 90 degrees to the jet (Microphone 5). (Note that this is the cruise Mach 0.8 freestream case). For the near field Kulite there is almost no dependency on mesh resolution - this is likely due to the predominant frequencies being quite low and easily resolved and the distance to propagate being short. The microphone case is more difficult as the signal needs to propagate approximately 7 jet diameters and the numerical dissipation of the coarser grids give overall lower noise levels (around 5dB) and a cut-off at a lower frequency. Nevertheless, this illustrates how Wall Modelled LES may be used in an industrial design setting where modest grids may be sufficient to capture the interaction noise source.

Moving onto Figure 14 which compares the same two virtual probes for the zero and 20 degree flap cases. There is a significant 10dB increase in the signal across the frequency range for the near field Kulite showing the increase in the noise source. This then propagates to the microphone with a 15dB increment at the very lowest frequencies and reducing to a 5dB increment at higher frequencies. In both cases the grid causes a drop off above 2kHz.

A rigorous comparison to experiment is difficult due to the high levels of rig noise and reverberation within the experimental facility. The rig is non-anechoic and in many runs the background noise was determined to be of a similar level to the jet noise. The most reliable probes are the near field Kulites as they have a much stronger signal than the microphones. To attempt to remove the rig noise we subtract a baseline. For both the experiment and CFD it is their corresponding case where we have a matched jet (i.e. the jet velocity matches the freestream) and the flap is at zero degrees. The baseline is effectively the airframe noise and the increment plotted is due to both jet shear noise and interaction noise. This is shown in Figure 14 for the same two probes. Somewhat disappointingly the CFD shows only a small increment for the near field Kulite at the lower frequencies whereas the experiment shows a significant

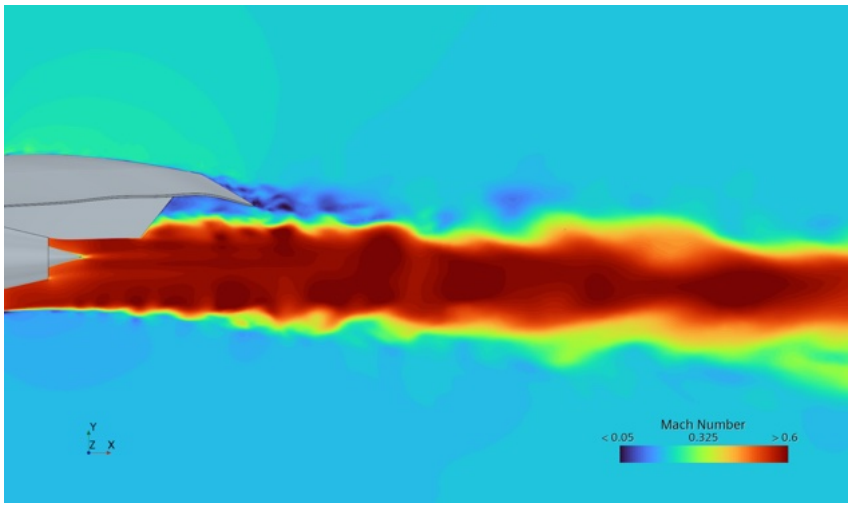

(a) 9M cells

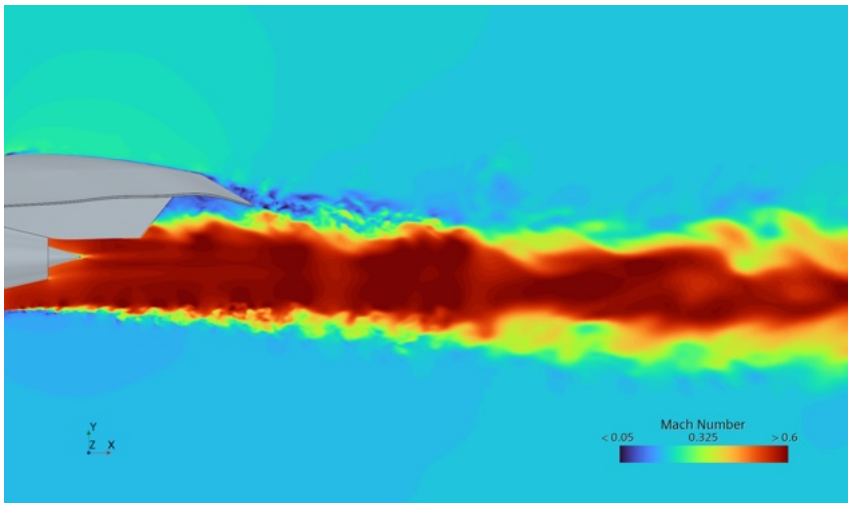

(b) 56M cells

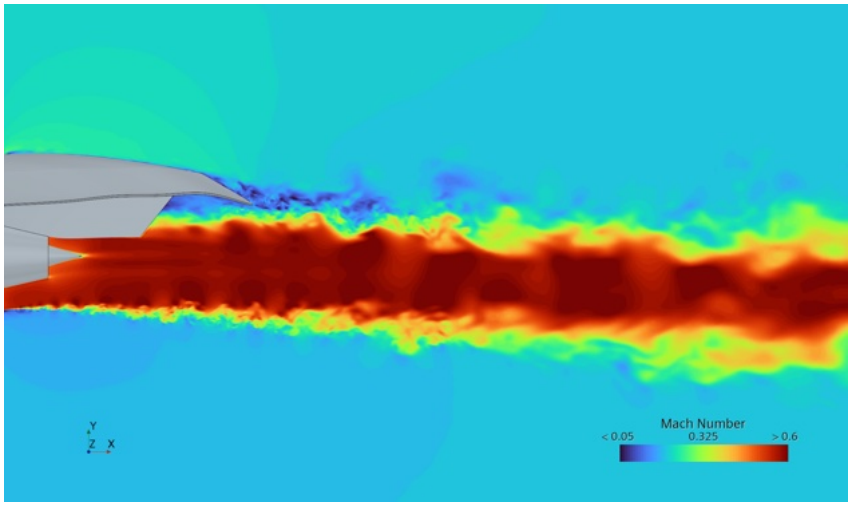

(c) 100M cells

Figure 7: Instantaneous Mach number jet centreline slice, 20 degree flap, $M_j = 0.6$, grid dependency

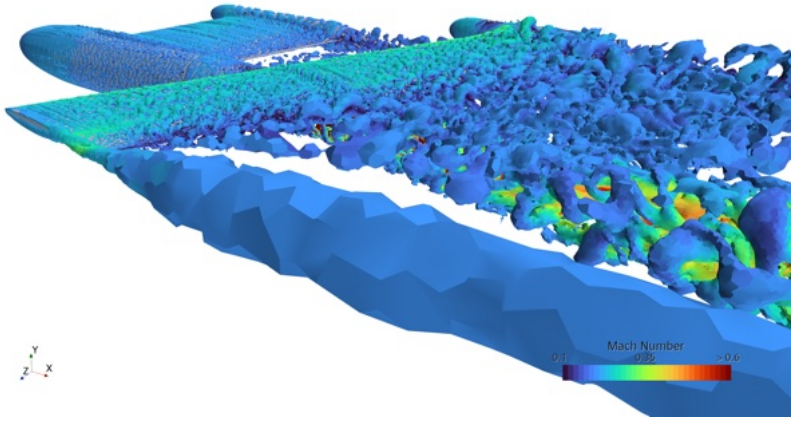

(a) 9M cells

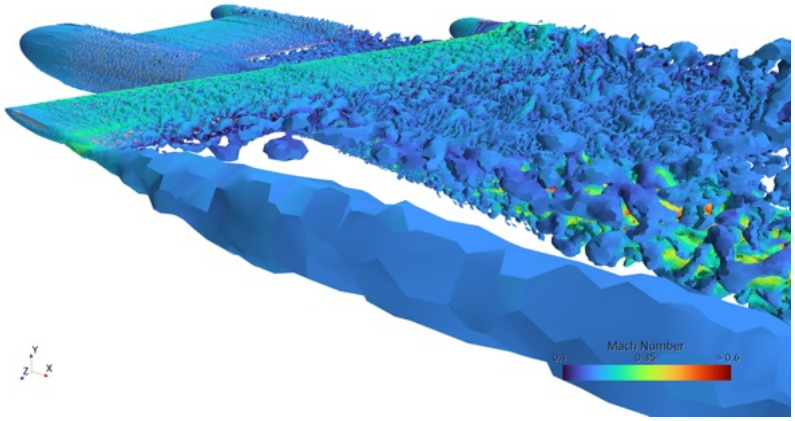

(b) 56M cells

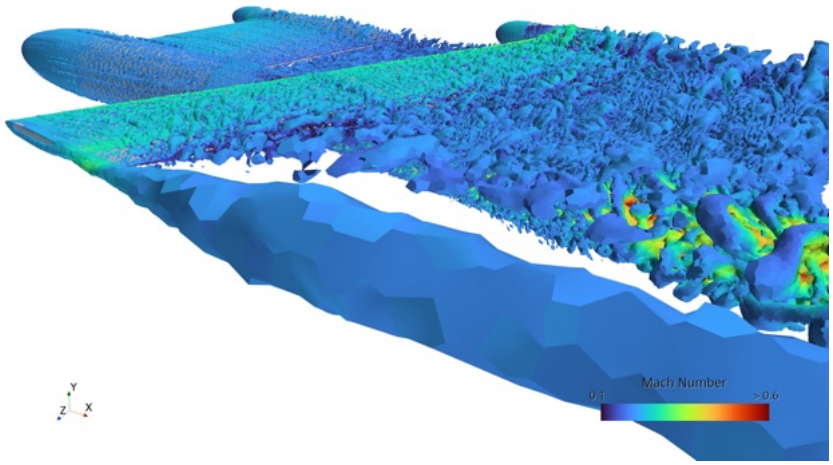

(c) 100M cells

Figure 8: Instantaneous Q-criterion, 20 degree flap, $M_j = 0.6$, grid dependency

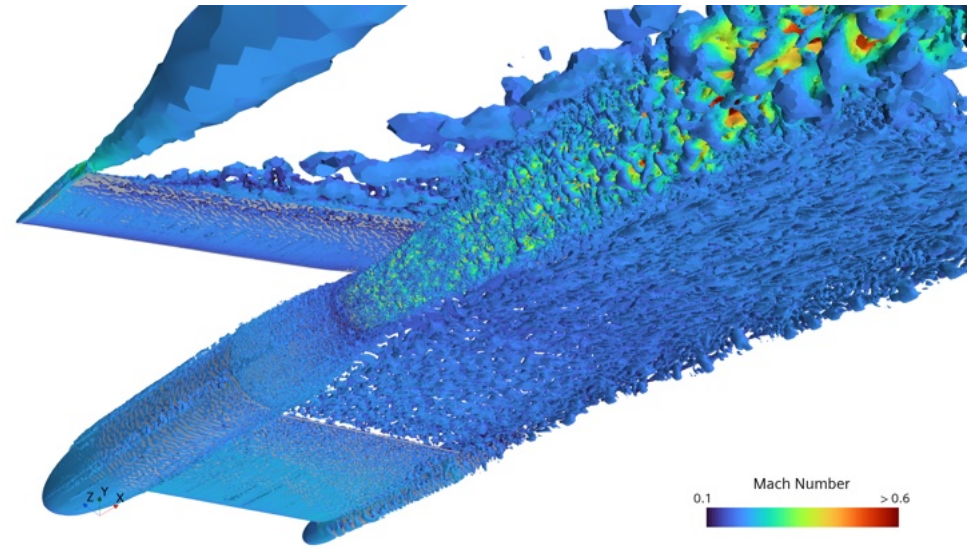

(a) underside

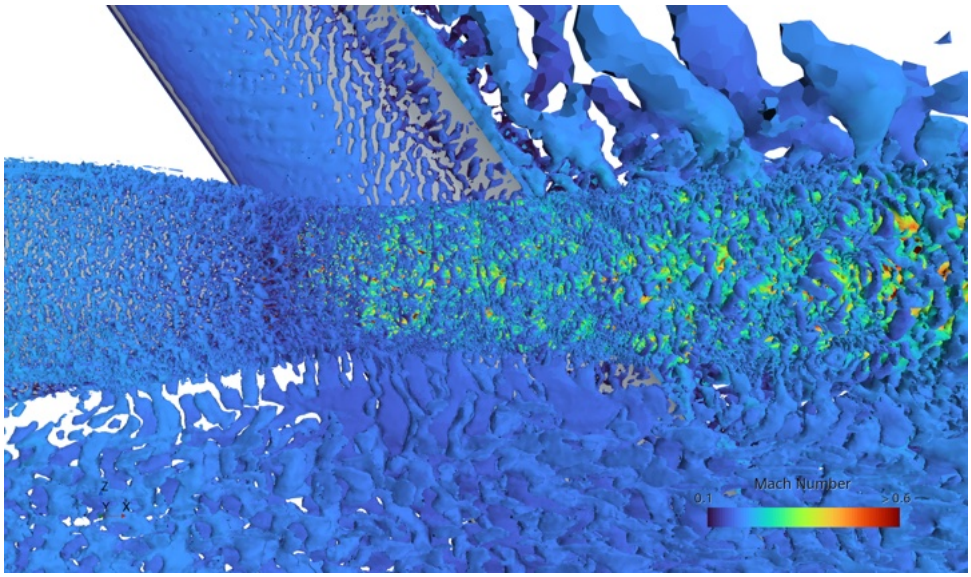

(b) jet view

Figure 9: Instantaneous Q-criterion, 20 degree flap, $M_j = 0.6$, 100M cells

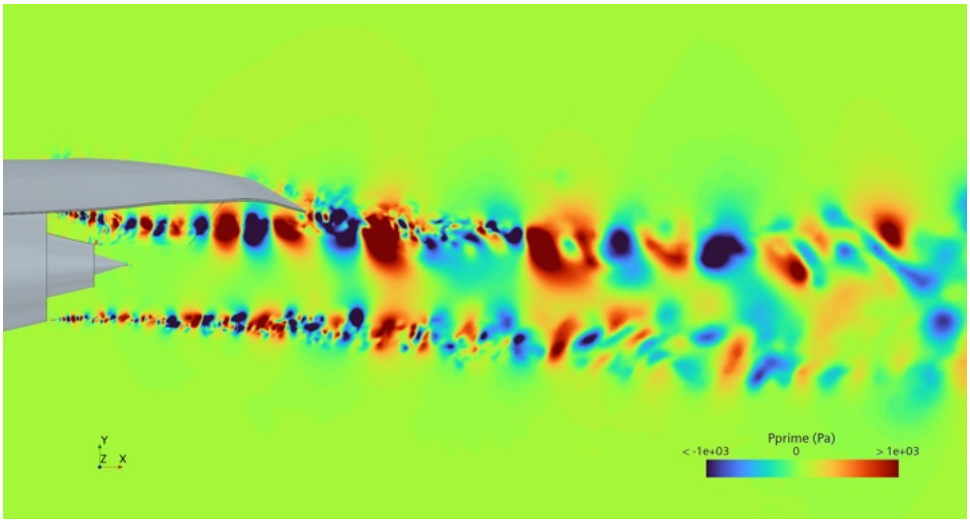

(a) jet vertical centreline cut

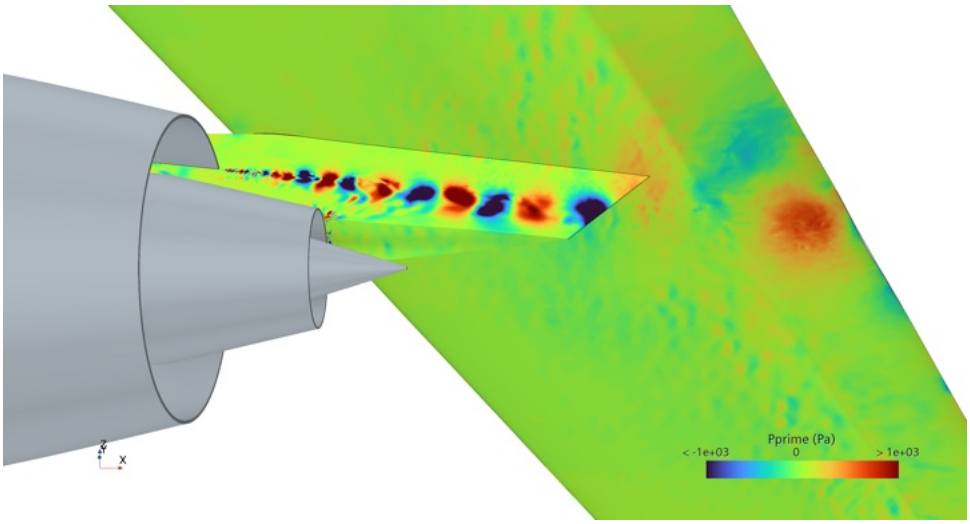

(b) wing and pylon

Figure 10: Instantaneous Pressure fluctuation around mean, 20 degree flap, $M_j = 0.6$, 56M cells

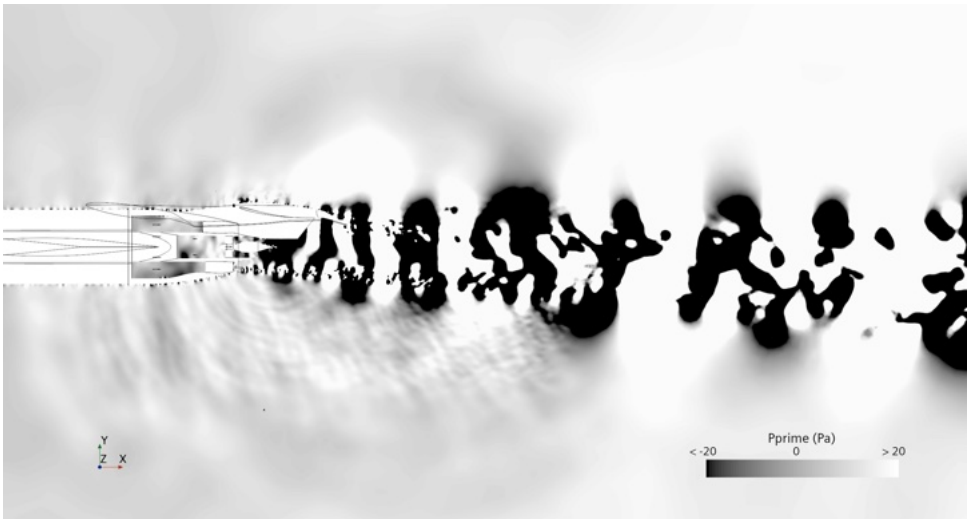

(a) jet vertical centreline cut acoustic perturbations (view along wing)

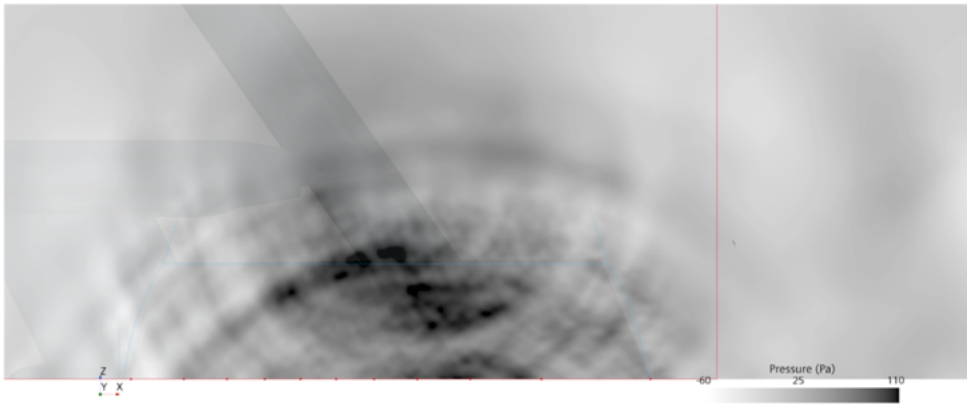

(b) propagation to microphone array (view normal to wing)

Figure 11: Acoustic propagation, 20 degree flap, $M_j = 0.6$, 56M cells

30dB. Surprisingly at the higher frequencies the CFD shows good agreement with experiment. For the midfield 90 degree microphone (Figure 14b), the CFD predictions again show little increment at low frequencies - and in this case is in agreement with experiment. The CFD somewhat overpredicts the experiment in the mid range frequencies and then drops off due to numerics at the higher frequencies. The shape of the spectra from the CFD is consistent across the two probes. Comparisons for other probes and locations are similarly inconclusive.

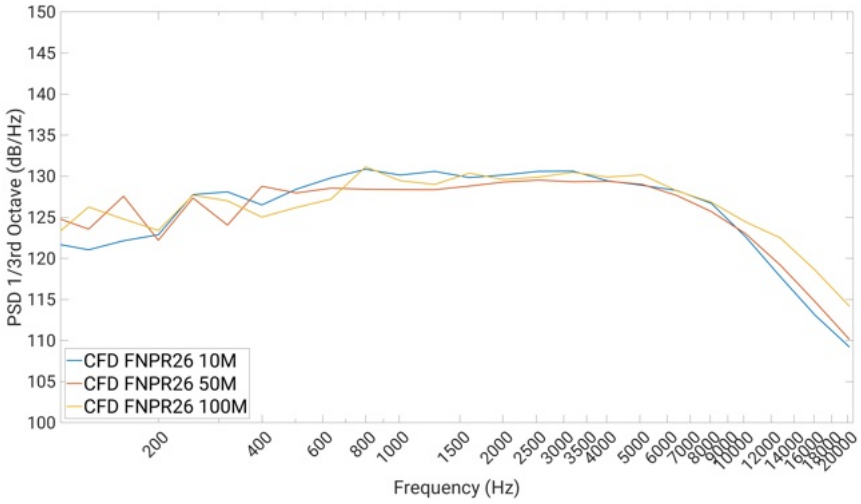

(a) Kulite 4 (flap TE underside)

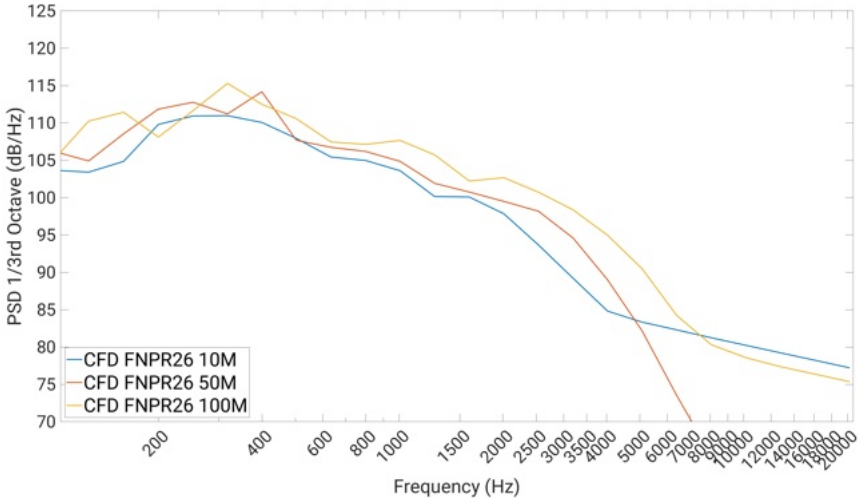

(b) Microphone 5

Figure 12: Mesh density sensitivity, 0 degree flap, NPR=2.6 ($M_f = 0.8$)

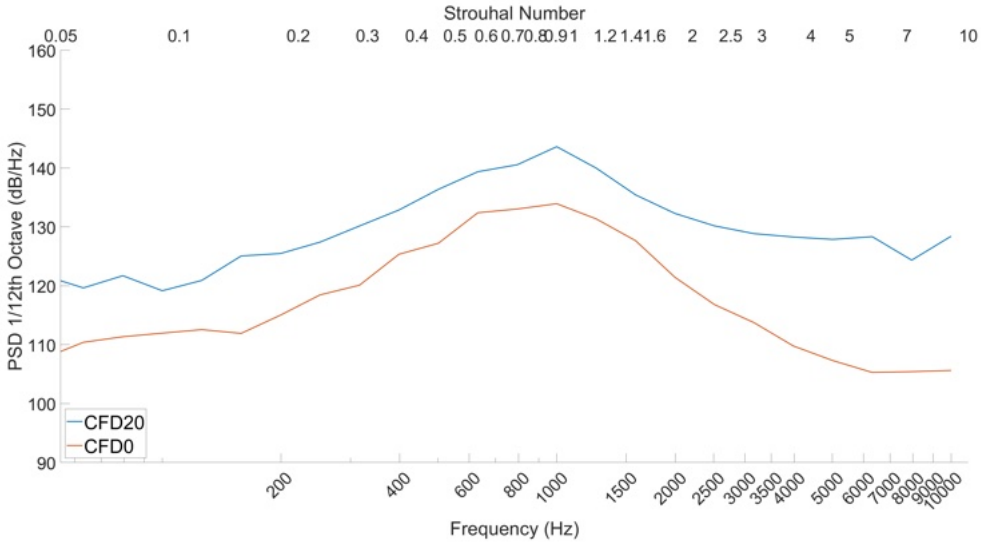

(a) Kulite 4 (flap TE underside)

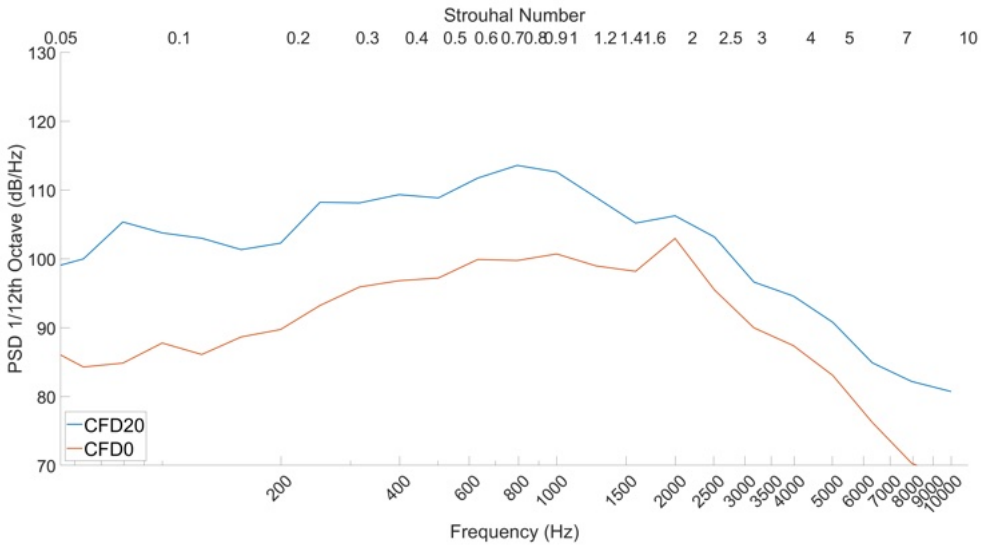

(b) Microphone 5 (90 degrees)

Figure 13: Jet Flap Interaction, $M_j = 0.6$, zero deg flap (CFD0) and 20 degree flap (CFD20)

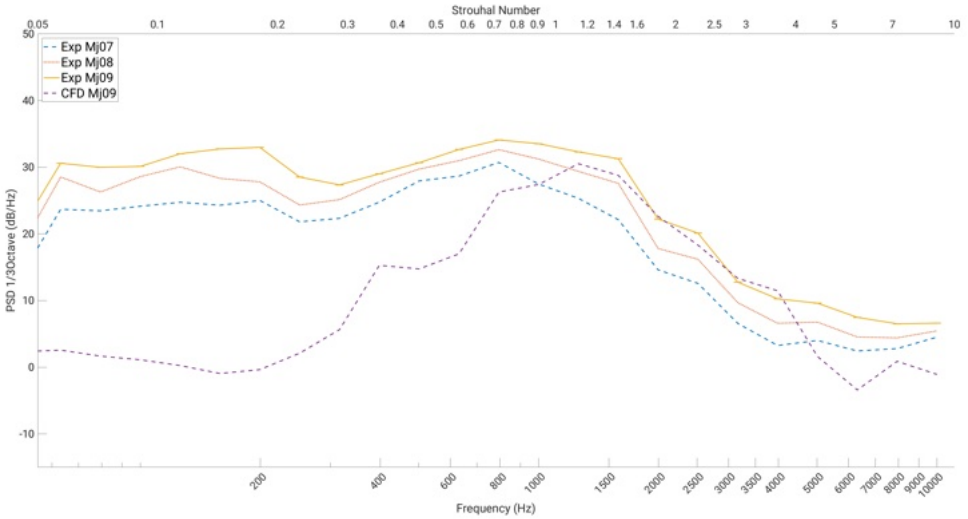

(a) Kulite 4

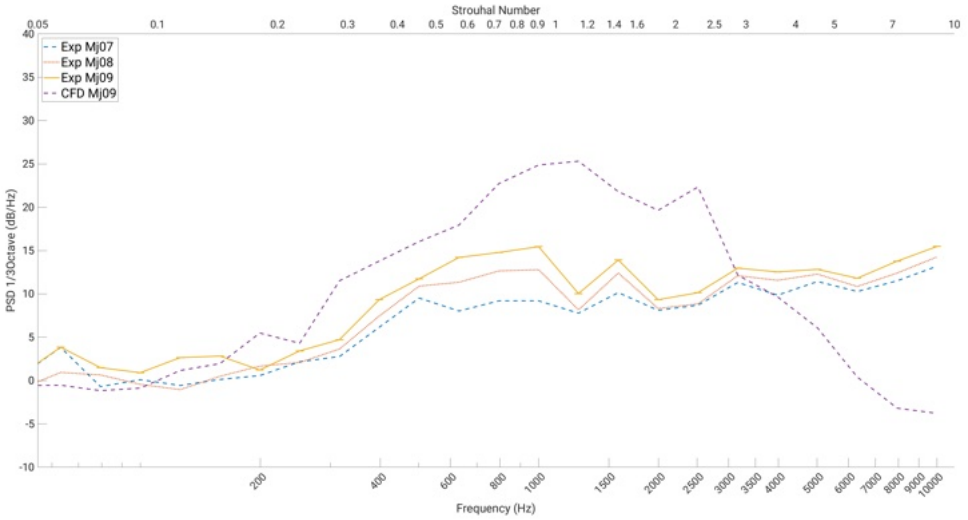

(b) Microphone 5

Figure 14: Jet noise increment, comparison with experiment, $M_j = 0.9, M_f = 0.2$

3 High Lift Common Research Model

The previous simulations have realistic flight and jet conditions, but the geometry is rather simplified compared to a modern transport aircraft. In particular, the flap is not slotted and the wing does not have a slat. One way of obtaining full geometric airframe and engine fidelity is to undertake a full scale flight test. In the past this would have involved flying over an instrumented microphone array, but to provide flexibility and knowledge of acoustic sources future tests may use an instrumented airframe with microphones mounted on the fuselage and wing. The CFD presented here replicates this future use case by simulating the NASA Common Research Model (CRM) with a modern compact nacelle and realistic intake and jet conditions. The CRM is a generic jet transport aircraft with characteristics similar to a Boeing 777. It was originally defined for CFD studies of drag prediction in cruise, and this is referred to here as the High Speed (HS) CRM. It was later adopted for landing cases by adding a high lift system, and this is referred to here as the High Lift (HL) CRM. The openly available geometry has a flow through nacelle, and for this work a representative UHBR powerplant with intake, exhaust, pylon and a compact nacelle was adopted with appropriate intake mass flows and exhaust temperature and pressures.

The CFD virtual microphones are mounted in a similar position to the ARA tests: on the flap to determine near field noise sources and on the fuselage to determine the mid-field. An advantage of the CFD is that the resolved jet noise sources can be propagated to the far-field to also determine far-field noise and how this correlates with the mid and near field. Two cases are simulated: Take Off (TO) using the High Lift CRM geometry with modifications to the flap and slat settings to change from the published landing configuration to a TO configuration; Cruise using the published High Speed CRM geometry. For brevity only the High Lift case is reported here.

3.1 Geometry

The full scale aircraft has a wing span of 58.76m with a reference area of 383.74m^2, giving an aspect ratio of 9.0. The Mean Aerodynamic Chord is 7.01m. The High Lift case has the slat angle set to 22 degrees and the flap angle to 25 degrees. As compared to the simplified geometry cases where the H/D was 0.478 (see Figure 2), in this case it has increased to 0.685 and hence a weaker Jet Flap Interaction would be expected.

3.2 Test Conditions

Calculations were run for sea level conditions with a Mach number of 0.25 and an angle of attack of 5.6 degrees. The viscosity was altered to match the Reynolds number of existing High Lift CRM wind tunnel tests with a value of 5×10^6 based on Mean Aerodynamic Chord. Realistic nozzle pressures and temperatures were used for the primary and secondary jet streams and the intake mass flow was set to match the exhaust mass flow.

3.3 Mesh

Mesh design and parameters were carried over from the previous simplified geometry 56M cell case. The use of anisotropic quad surface meshes was important to capture efficiently the high streamwise gradients at the intake, jet nozzles, slats and flaps (see Figure 15a). Unlike most CFD simulations of the High Lift model that aim to predict the flow around the aircraft and hence the lift coefficient, our aim is that the airframe provides realistic flow conditions to the jet. Consquently much of the mesh is used to resolve the jet rather than the airframe. For example, based on MAC, the wing spacing varies from 1.5% at mid-chord down to 0.125% at the leading and trailing edges. Hence, our surface mesh is relatively coarse compared to pure aerodynamic studies. The previous calculations' prism layer design was used with 13 layers and a target near wall thickness to achieve a near wall cell centre y^+ of 40-100. The achieved y^+ is shown in Figure 15b. The highest values are around 150 in the intake and slats and is due to high accelerations (suction), for an aerodynamic simulation this should be further improved but is sufficient here as the important nacelle is within the target range.

A series of nested refinements of the polyhedra mesh were applied (Figure 16) with the smallest cells being 0.5% of the secondary jet stream diameter (approximately half the MAC) and the largest cells being 10% of the jet diameter and extending 30 diameters downstream.

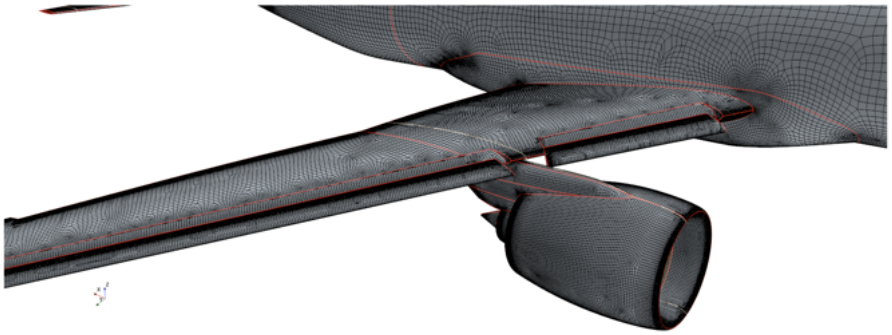

(a) mesh

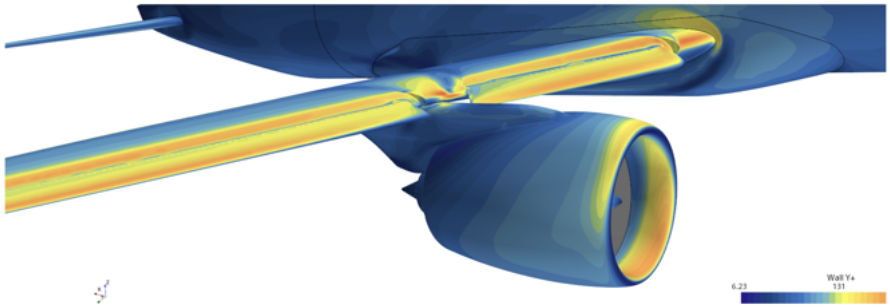

(b) near wall y^+

Figure 15: HLCRM, surface

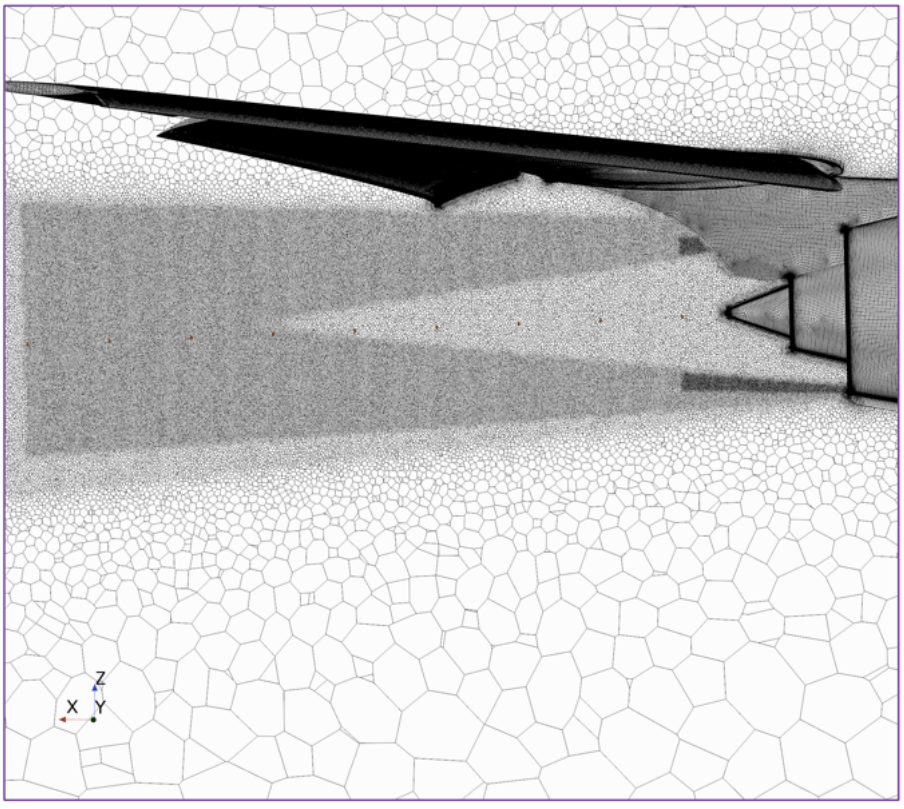

Figure 16: HLCRM, volume mesh

3.4 Flow Field

Instantaneous flow visualisations of Mach number and Q-criterion are shown in Figures 17 and 18. Quantitatively these are similar to the earlier simplified geometry, but the increased complexity of the problem with the same cell count has had an impact. For example, there is much less resolution of unsteadiness on the aircraft surface due to the reduced surface resolution. The unsteadiness is limited to the flaps and slats and the undersurface of the Horizontal Tail Plane that is set to zero angle of attack but has a much higher effective angle due to the flap downwash. Of more importance is the unrealistic ring like structures initially formed in the jet shear layer that then rapidly breakdown into turbulence – again more resolution is required in this small region. It should be noted that with modern engines that have similar core and bypass stream speeds, then as the speed of sound in the core is higher due to its higher temperature, the core Mach number is lower than bypass stream Mach number (Figure 17).

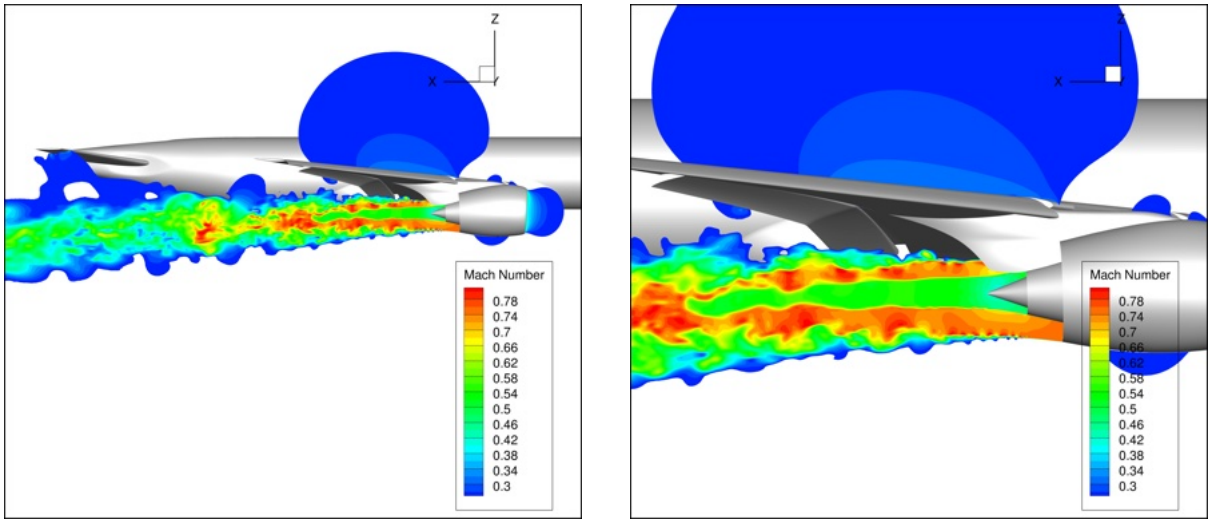

(a) Mach number slice jet centreline

(b) Mach number slice jet centreline detail

Figure 17: HLCRM, Mach number

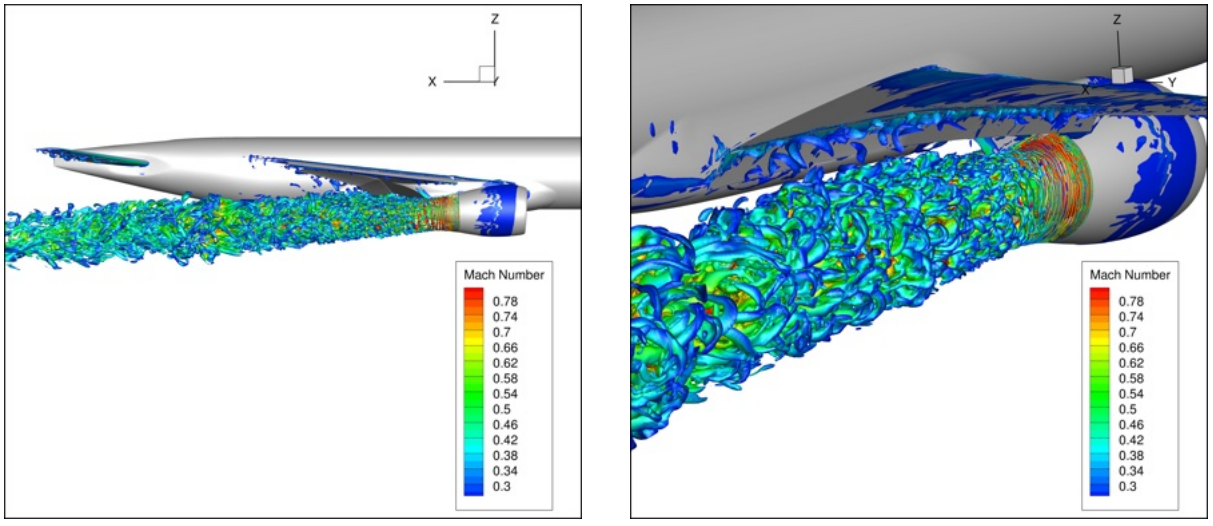

(a) side view

(b) rear view

Figure 18: HLCRM, Q-criterion coloured by Mach number

3.5 Acoustic Propagation

Shadowgraph techniques are used in experimental measurement to emphasise density gradients from waves in the flow. This can be simulated using the Laplacian of the density field[2] and is shown in Figure 19. Even with the larger H/D parameter, Jet Flap Interaction is observed as spherical waves centred on the flap trailing in both the side and top views. The JFI is more visible in the forward arc, whilst in the rearward arc these are masked by the more chaotic jet mixing noise. As the waves move towards the edge of these images the mesh becomes coarser and rapidly damps them. It is interesting to note the waves propagating forward from the engine inlet. There is obviously no rotating fan modelled in these calculations, instead it is likely that the fixed mass flow boundary condition at the fan face is creating these spurious waves.

As mentioned earlier, virtual 'Kulite' and 'microphone' probes were placed on the wing and fuselage in the equivalent positions to the simplified geometry (Figure 20 and 20c). The lower line of fuselage microphones mainly on the wing/body fairing are the best in terms of avoiding wing shielding, but the upper line that is on the cabin sidewall is more practical in terms of installation on a real flight test aircraft.

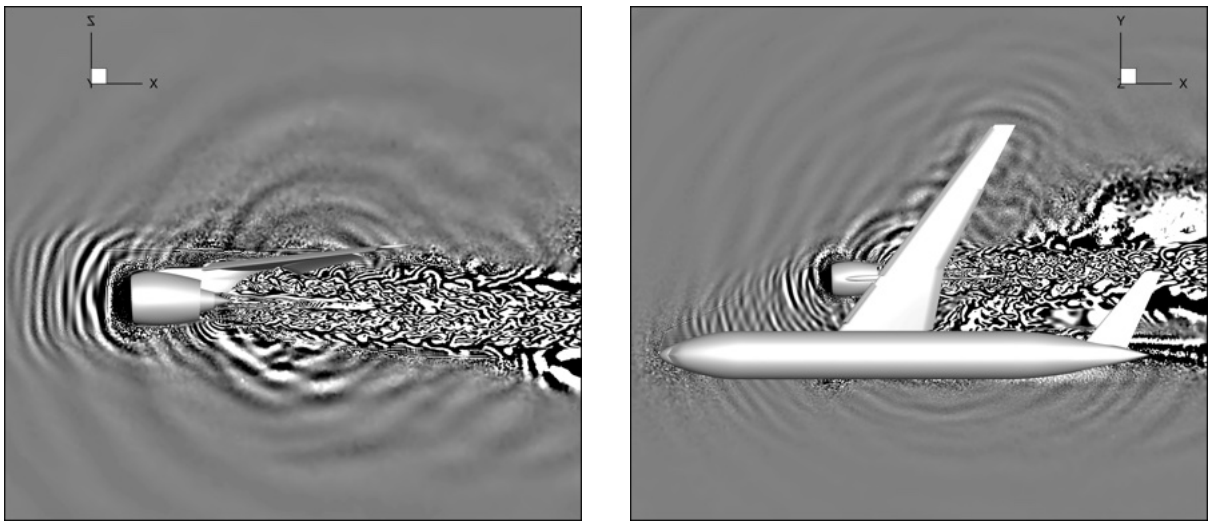

(a) side view (b) top view

Figure 19: HLCRM, simulated shadowgraph

We might expect that the upper microphones near to 90 degrees from the jet would be shielded by the wing and would have lower pressure fluctuations. The CFD shows the opposite trend (Figure 21) with the upper microphone being considerably noisier. This appears to be due to the increased levels of airframe noise for the upper microphone. Figure 22 shows flow visualisation of turbulent structures and the locations of the upper and lower microphones. Because of the high angle of attack there is considerable turbulence generated on the wing upper surface, around the pylon intersection and on the fuselage. Whereas on the lower surface the favourable pressure gradients suppress large scale turbulence (the Wall Modelled LES cannot resolve the very finest scales of turbulence). For a flight test aircraft to assess jet noise, then it is preferable that the microphone array be located on a line under the wing.

4 Conclusions

This paper has documented Wall Modelled LES of a simplified geometry and a realistic aircraft geometry for the study of Jet Flap Interaction.

The simplified geometry showed that WMLES on modest grids is capable of resolving realistic turbulent structures and so becomes affordable to study a number of test cases. The CFD shows a clear increment in noise at both the near field and mid field location when changing from a zero degree flap to 20 degree flap. There is a significant 10dB increase in the signal across the frequency range for the near field Kulite on the flap underside. This source then propagates to the microphone with a 15dB

[2]Function 197 from Plot3D, circa 1989

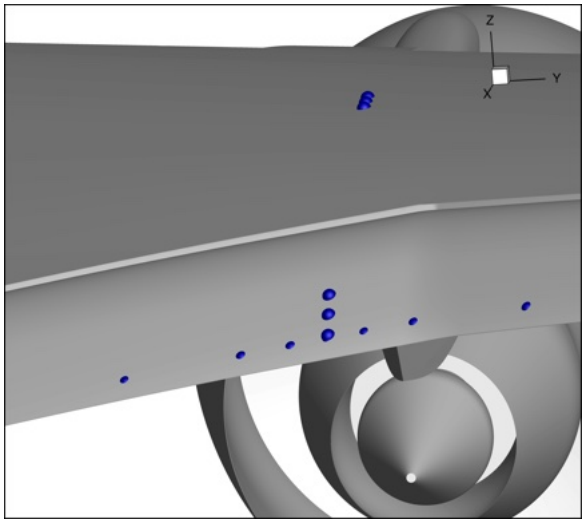

(a) wing/flap upper

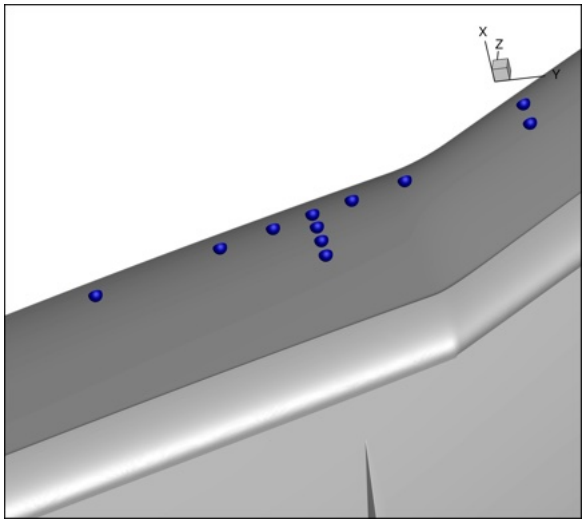

(b) wing/flap lower

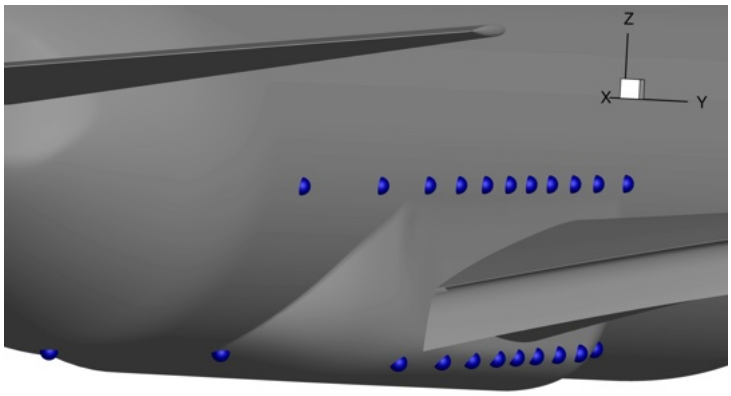

(c) Microphone locations

Figure 20: HLCRM Flight Test Aircraft, simulated Kulites and microphones

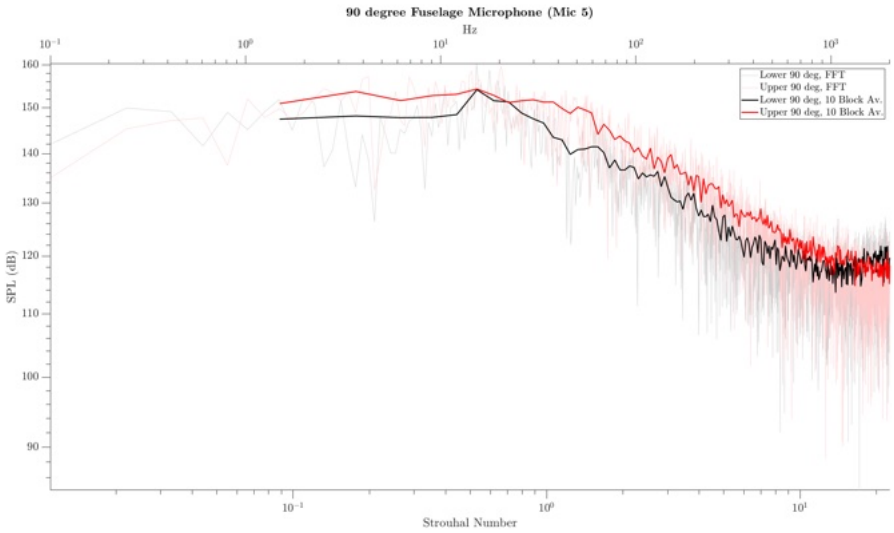

Figure 21: Microphone 5 (90 degrees) red upper, black lower microphone

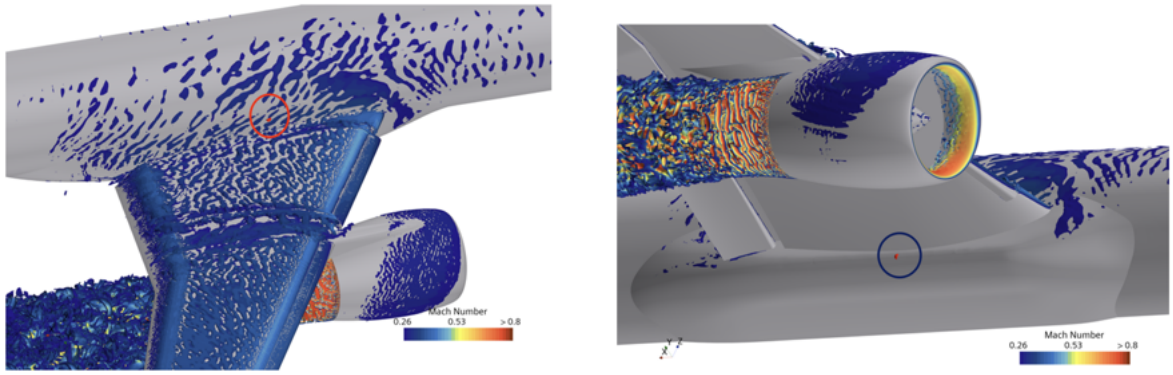

(a) flow field near upper 90 degree microphone (b) flow field near lower 90 degree microphone

Figure 22: HLCRM Flight Test Aircraft, flow near 90 degree microphone 5

increment at the very lowest frequencies and reducing to a 5dB increment at higher frequencies. Direct comparison with experimental data was not possible due to the high level of rig noise in the facility. Instead the increment in noise when compared to the respective baseline with zero flap and matched jets were compared. For the near field the increment is much larger for the experiment at low frequencies but there is good agreement at mid to high frequencies. For the mid-field microphone the large low frequency increment for the experiment has disappeared and there is reasonable agreement between simulation and experiment across the frequency range.

The realistic installed aircraft was based on the High Lift Common Research model modified to a take off configuration and with the addition of a modern UHBR gas turbine. Similar flow and acoustics behaviour to the simplified case was observed, although it is recommended that finer grids be employed to resolve both the airframe and jet turbulence adequately. Noise sources due to Jet Flap Interaction were observed in simulated shadowgraph images. Virtual probes were added in a similar position to the simplified geometry and these showed that microphones along the cabin above the wing are likely to be contaminated by airframe noise and it is recommended that microphones should instead be placed under the wing.

5 Acknowledgements

This paper acknowledges the use of the Lovelace HPC service at Loughborough University to provide computing resources. We would also like to acknowledge the invaluable input of other partners in the ODIN project including Cranfield University, University of Cambridge and the Aircraft Research Association.

References

[1] Jente, C., Pott-Pollenske, M., Boenke, D., Buescher,A. and Goldhahn,I., "Experimental Investigation of Jet-Flap-Interaction Noise Sensitivity due to varying flap parameters at a UHBR Engine/High-Lift-Wing installation," American Institute of Aeronautics and Astronautics, 2018. https://doi.org/10.2514/6.2018-3788.

[2] Angelino, M., Moratilla-Vega, M.A., Howlett, A., Xia, H. and Page, G.J., "Numerical Investigation of Installed Jet Noise Sensitivity to Lift and Wing/Engine Positioning," AIAA 2019-2770. 25th AIAA/CEAS Aeroacoustics Conference. May 2019. https://doi.org/10.2514/6.2019-2770

[3] Angelino, M., Fernández-Yáñez, P., Xia, H. and Page, G.J., "Large-Eddy Simulation with Modeled Wall Stress for Complex Aerodynamics and Stall Prediction" *AIAA Journa*l 2021 59:4, 1225-1237 https://doi.org/10.2514/1.J059481